

Ionic and Electronic Transport in Ag₂S Nanocrystal–GeS₂ Matrix Composites with Size-Controlled Ag₂S Nanocrystals

Robert Y. Wang, Ravisubhash Tangirala, Simone Raoux, Jean L. Jordan-Sweet, and Delia J. Milliron*

The Ag-Ge-S system is among the best-performing active materials for a new class of high-performance electronic memory known as programmable metallization cells.^[1,2] Memory switching in a programmable metallization cell relies on the electrochemical formation and dissolution of an electronically conducting filament within a solid electrolyte. In the Ag-Ge-S system, this electrochemical process is facilitated by the transport of both Ag⁺ ions and electrons. Consequently, it is important to understand how the ionic conductivity and electronic conductivity relate to the structure of the Ag-Ge-S system. However, this understanding is hampered by the ill-defined morphology of Ag-Ge-S, which consists of an amorphous Ge-rich matrix with embedded Ag-rich nano-inclusions of random size, shape, and interparticle spacing.^[1,2] We circumvent these morphological ambiguities by controlling these structural variables with our recently developed nanocomposite formation technique.^[3] We create Ag₂S nanocrystal–GeS₂ matrix composites and demonstrate that their ionic and electronic properties can be systematically controlled by varying the diameter of the Ag₂S nanocrystals. We also observe an ionic conductivity enhancement relative to pure Ag₂S and (GeS₂)_{0.5}(Ag₂S)_{0.5} glass. Additionally, the thermal phase transition of Ag₂S into its superionic phase exhibits differences in thermal hysteresis and transition temperature when comparing the composites to pure Ag₂S.

The combined structural control and chemical composition flexibility of our nanocomposite formation technique will allow the careful study of structure-property relationships in many important nanocomposite systems. The flexibility of the nanocomposite fabrication is enabled by a modular formation process in which nanocrystals and chalcogenidometallate (ChaM) clusters are independently synthesized. After assembling the nanocrystals into a thin film, the ChaM clusters are intercalated into the interstitial space between nanocrystals. The ChaM clusters are then converted into an inorganic matrix

by thermal decomposition. This process allows the control of nanocrystal size, shape, and interparticle spacing within the matrix material (Figure 1).^[3] The flexibility of the nanocomposite's chemical composition arises because of the wide available selection of nanocrystals^[4] and ChaM clusters.^[5] A detailed report on the structural characterization of these nanocomposites can be found in our prior publication.^[3]

As a first application of this approach to technologically-relevant nanocomposites, we created Ag₂S nanocrystal–GeS₂ matrix composites with controlled structure and investigated their corresponding charge transport properties. GeS₂ is an amorphous solid electrolyte that conducts Ag⁺ ions^[6,7] whereas Ag₂S is a crystalline solid that conducts both Ag⁺ ions and electrons.^[8] In addition to studying microstructure effects on charge transport, this composite platform allowed us to investigate size-effects on phase transitions. Ag₂S experiences a solid-solid crystal phase transition at 177 °C. Accompanying the transition from the low temperature Ag₂S phase (i.e. acanthite) into the high temperature Ag₂S phase (i.e. argentite) is a large increase in both electronic and ionic conductivity. Argentite Ag₂S has unusual conductivity properties; it has an ionic conductivity comparable to the best solid electrolytes, but the overall charge transport is predominantly electronic.^[8]

To make the composite we used spherical Ag₂S nanocrystals with octadecylamine surface ligands and (N₂H₄)_x(N₂H₅)₄Ge₂S₆ chalcogenidometallate (ChaM) clusters.^[3,5,9] The Ag₂S nanocrystal diameter in the composite was controlled to be between ~4.3–11.6 nm by varying the initial nanocrystal synthesis. Based on our previous work, we estimate the thickness of the GeS₂ matrix separating the individual Ag₂S nanocrystals to be 0.7 nm.^[3] Since the ChaM ligand exchange occurred after nanocrystal film assembly, this GeS₂ thickness should be equivalent for all nanocrystal sizes (Figure 1). For comparative purposes, pure Ag₂S thin films were prepared by sulfidizing Ag films. These Ag films were prepared by thermal evaporation onto amorphous SiO₂ substrates.

The x-ray diffraction (XRD) pattern of a Ag₂S nanocrystal–GeS₂ matrix composite consists of diffraction peaks superimposed onto a broad hump (Figure 2). At room temperature, most of the observed peaks correspond to acanthite Ag₂S whereas the broad hump can be ascribed to the amorphous GeS₂ matrix which does not diffract. The additional diffraction peak at 24° indicates that portions of the Ag₂S and GeS₂ reacted to form Ag₂GeS₃, which has been observed in prior studies on the Ag-Ge-S material system.^[1] After heating to 200 °C, the phase transition from acanthite Ag₂S to argentite Ag₂S is evident. Upon cooling back to room temperature, the original acanthite Ag₂S XRD pattern returns. No significant changes in the diffraction

Prof. R. Y. Wang, Dr. R. Tangirala, Dr. D. J. Milliron
The Molecular Foundry
Lawrence Berkeley National Laboratory
Berkeley, CA, 94720, USA
E-mail: dmilliron@lbl.gov
Prof. R. Y. Wang
Mechanical Engineering
Arizona State University
Tempe, AZ, 85281, USA
Dr. S. Raoux, Dr. J. L. Jordan-Sweet
IBM T. J. Watson Research Center
Yorktown Heights, NY 10598, USA



DOI: 10.1002/adma.201102623

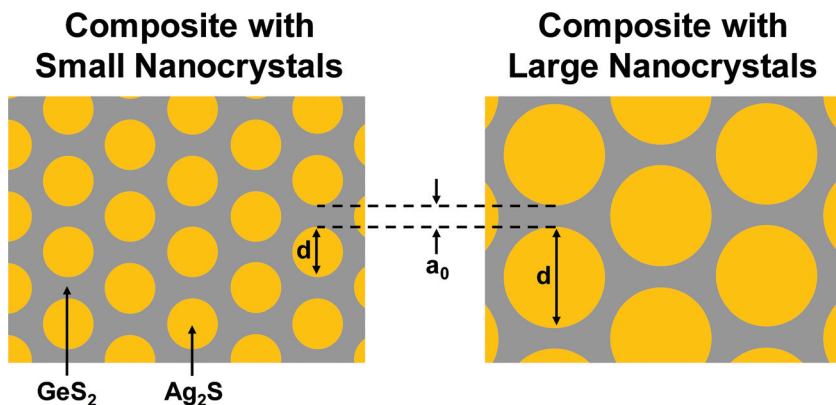


Figure 1. Cross-sectional schematics of the nanocomposites studied in this work. The composites consist of Ag_2S nanocrystals (yellow) embedded in an amorphous GeS_2 matrix (gray). The Ag_2S nanocrystal diameter, d , was varied from 4.3 nm to 11.6 nm. The interparticle spacing, a_0 , is ~ 0.7 nm and is the same for all nanocrystal diameters.

pattern or peak widths are observed during this thermal cycling process, which demonstrates that the GeS_2 matrix prevents the Ag_2S nanocrystals from sintering into larger crystallites. Several XRD differences are observed when comparing pure Ag_2S and composites with varying nanocrystal diameters (Figure 3). The pure Ag_2S sample shows texturing, which likely originates from the preferential orientation of the Ag film that was sulfidized.^[10] No texturing is observed in the nanocomposites because of the randomized nanocrystal orientation during film assembly. As expected based on the crystallite size, the diffraction peaks get broader as the Ag_2S characteristic length is decreased.

We examined the Ag_2S phase transition by varying temperature in situ under the x-ray beam (Figure 3). The sharpness

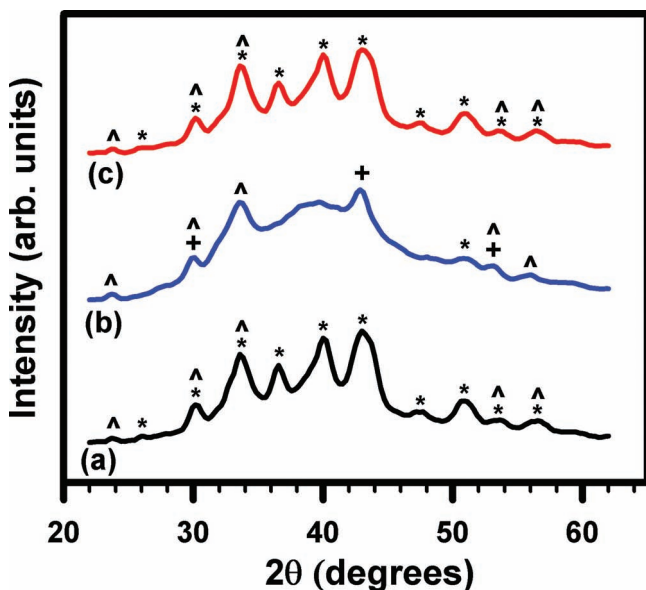


Figure 2. X-ray diffraction patterns ($\lambda = 1.797$ Å) of a 8.7 nm Ag_2S nanocrystal– GeS_2 matrix composite taken at (a) room temperature, (b) heated to 200 °C, and then (c) cooled to room temperature. The peaks labeled with *, +, and ^ correspond to the acanthite Ag_2S (JCPDS 00-014-0072), argentite Ag_2S (JCPDS 01-076-0134), and Ag_2GeS_3 (JCPDS 00-033-1180), respectively.

of the acanthite-argentite phase transition decreases as the Ag_2S characteristic length is decreased. This gradual phase transition explains why a residual acanthite peak is observed at 200 °C for a composite containing 8.7 nm Ag_2S nanocrystals (Figure 2b). The phase transition becomes so gradual that despite reaching 228 °C, no clear transition is observed in the composite with 5.9 nm Ag_2S nanocrystals. In addition, the transition temperature of the composites is lower than that of bulk Ag_2S and a thermal hysteresis of ~ 7 °C and ~ 20 °C is observed in the pure Ag_2S thin film and composites, respectively. These changes in phase transition characteristics are also reflected in our charge transport measurements (see Supporting Information). Phase transition hysteresis in bulk silver chalcogenide compounds has

been previously reported and the density difference between the two phases plays a key role in the transition.^[11,12] Size-effects on solid-solid phase transitions have been previously observed in other works,^[13–16] and are believed to arise from interface defects and changes in surface energy. Recently, a more dramatic hysteresis enhancement at small sizes was shown to stabilize the high temperature superionic phase of AgI near room temperature.^[14]

We used the morphological control of our composites to investigate the effect of nanocomposite structure on ionic conductivity, σ_i , and electronic conductivity, σ_e . To measure these properties, we used a combination of impedance spectroscopy and dc measurements.^[17,18] Platinum electrodes, which block Ag^+ ion transport, facilitate the differentiation of electronic from ionic transport.^[17,18] The contribution of electrons to the overall charge transport can be quantified by the electronic transference number, t_e , which is: $t_e = \sigma_e / (\sigma_e + \sigma_i)$. We measured these properties from 130 °C to 230 °C for a pure Ag_2S thin film and nanocomposites containing nanocrystals of diameters 4.3 ± 0.8 nm, 7.0 ± 1.4 nm, and 9.3 ± 2.8 nm (Figure 4). We estimate the Ag_2S volume fractions of these composites to be 47, 55, and 60%, respectively.^[19] A change in the slopes of the conductivity curves occurs near 175 °C, which we attribute to the Ag_2S phase transition. Over the temperature range studied, the electronic transference number ranges from 0.01–0.03, 0.10–0.18, and 0.17–0.28 for the 4.3 nm, 7.0 nm, and 9.3 nm nanocrystals, respectively. In the acanthite phase, the pure Ag_2S film has an electronic transference number of 0.90–0.93. We could not measure the ionic conductivity of the pure Ag_2S film in the argentite phase because the charge transport is predominantly electronic (i.e. $t_e \approx 1$).

As the Ag_2S nanocrystal size is increased, the electronic conductivity monotonically increases and approaches that of pure Ag_2S . At the phase transition temperature, the electronic conductivity curve of the pure Ag_2S thin film exhibits a change in slope and a one order of magnitude increase. In the composites, the GeS_2 matrix prevents the large increase in conductivity at the phase transition; instead a small increase in conductivity and a change in slope are observed. The effect of the GeS_2 matrix is especially pronounced in Figure 4c, which shows that

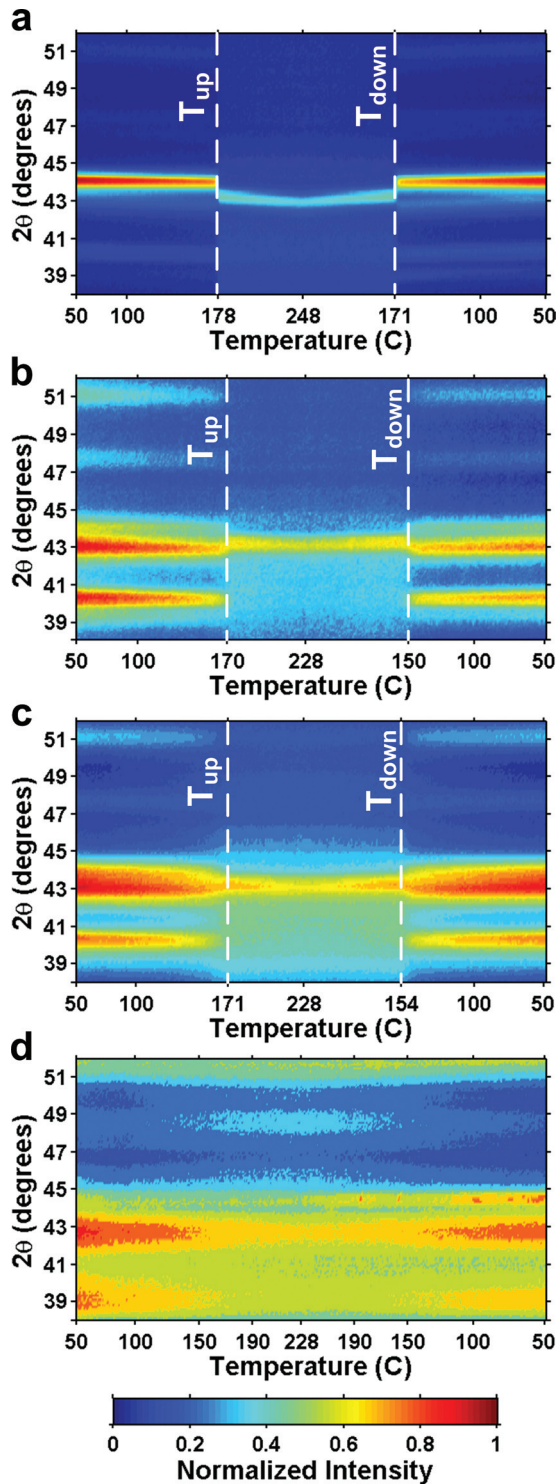


Figure 3. X-ray diffraction patterns of the nanocomposites and a pure Ag_2S thin film as the sample temperature is varied *in situ*. The 2θ peak intensity at each temperature is indicated by the color scale. The plots correspond to (a) a pure Ag_2S thin film (thickness = 256 nm); and Ag_2S nanocrystal– GeS_2 matrix composites with Ag_2S nanocrystal diameters of (b) $11.6 \text{ nm} \pm 1.9 \text{ nm}$, (c) $8.7 \text{ nm} \pm 1.7 \text{ nm}$, and (d) $5.9 \text{ nm} \pm 1.6 \text{ nm}$. The phase transition temperature during heating and cooling are labeled as T_{up} and T_{down} , respectively. The central tick mark on the temperature axis indicates the maximum temperature reached during the heating cycle.

the electronic transference number is ~ 1 for pure argentite Ag_2S , but only 0.01–0.28 for the nanocomposites. Hence, we can tune the balance between electronic and ionic transport, and the absolute electronic conductivity, through systematic variation of the Ag_2S particle size. This effect is derived from the variation in the volume fraction of the GeS_2 , which greatly hinders, but does not completely block, electronic transport.

The most striking aspect of our data is that the ionic conductivity of the nanocomposites exceeds that of both pure Ag_2S and $(\text{GeS}_2)_{0.5}(\text{Ag}_2\text{S})_{0.5}$ glass (Figure 4b). Studies show that the amount of free volume within a material's atomic structure can significantly affect ionic transport.^[20–22] Lattice contraction can decrease ionic conductivity,^[20] whereas ionic conductivity progressively increases for materials with lattice dilation,^[20] dislocation defects,^[21] and atomic disorder.^[22] For example, atomic disorder in CSZ ($\text{ZrO}_2 + \text{CaO}$) yielded an increased ion mobility and resulted in an ionic conductivity enhancement factor of $\sim 10^2$.^[22] It is possible that a similar effect may be happening in our GeS_2 matrix. It is well-documented that precursor decomposition processes generally do not yield fully dense materials.^[23] Hence the GeS_2 matrix, which is created by decomposition of the ChaM clusters, may have additional free volume and a corresponding enhanced ionic conductivity. We note that heterogeneous doping is often used to explain the observed ionic conductivity differences between nanomaterials and bulk materials. Heterogeneous doping can increase the ionic conductivity of nanomaterials by interfacial charge carrier accumulation or it can decrease the ionic conductivity of nanomaterials by interfacial charge carrier depletion.^[24–26] A hallmark characteristic of heterogeneous doping is that its effect becomes more pronounced as the interface density increases; however we observe the opposite trend. As the interface density of our composites increases, their ionic conductivity decreases toward that of the bulk material. This means that although heterogeneous doping may be present, another more dominant effect is taking place as we change the Ag_2S nanocrystal size.

As the Ag_2S nanocrystal diameter changes from 4.3 to 9.3 nm (which correspond to Ag_2S volume fractions of 47% and 60%, respectively) we observe a substantial ~ 10 -fold increase in ionic conductivity. This relative change is similar to that reported in literature for $(\text{GeS}_2)_{1-x}(\text{Ag}_2\text{S})_x$ glasses, in which a ~ 10 -fold increase in ionic conductivity is observed as x is increased from 40% to 55%.^[7] Since the observed changes of ionic conductivity in our nanocomposites and $(\text{GeS}_2)_{1-x}(\text{Ag}_2\text{S})_x$ glasses are so similar, this may mean that these trends have similar origins. The simplest explanation would be to consider a mean field approximation and conclude that the Ag_2S nanocrystals are more ionically conductive than the matrix. However, the ionic conductivity of $(\text{GeS}_2)_{1-x}(\text{Ag}_2\text{S})_x$ glasses have a super-linear dependence on x ,^[7,27,28] which mean field approximations cannot explain. Several models^[29–31] have been proposed to explain this trend. These models suggest that either the ion mobility changes^[29,30] or that a changing fraction of the ions contribute to charge transport.^[31]

Due to Ag migration from the Ag_2S nanocrystals into the matrix, the nanocomposite's matrix is expected to have a Ag–Ge–S composition. As there are two different glass-forming regions with very different atomic arrangements in the Ag–Ge–Se phase diagram (which is analogous to Ag–Ge–S phase diagram), the

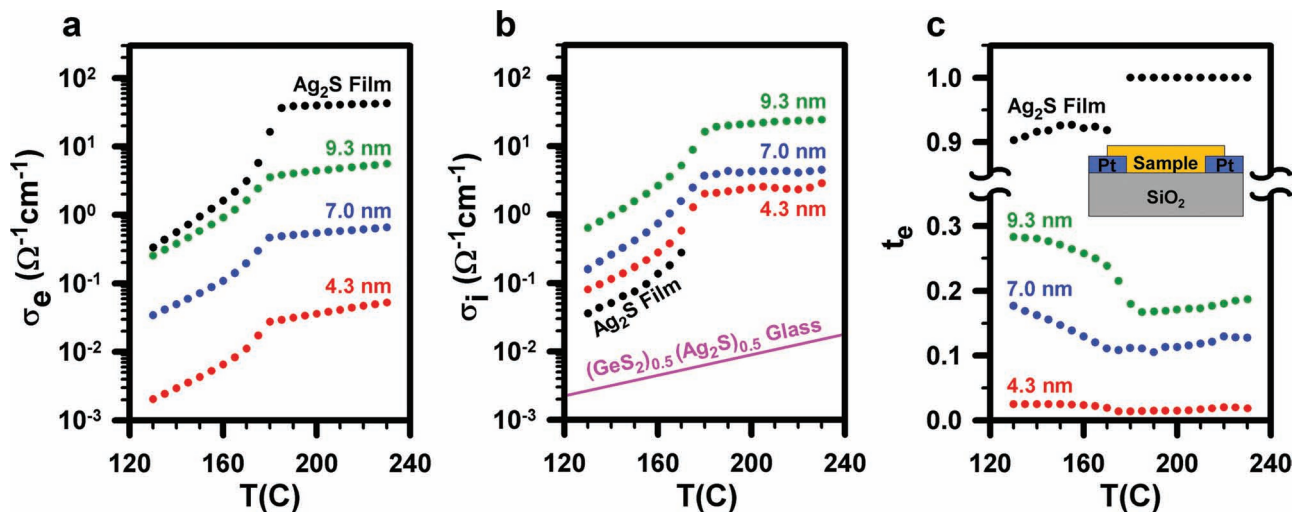


Figure 4. The (a) electronic conductivity, (b) ionic conductivity, and (c) electronic transference number of the nanocomposites, pure Ag₂S thin film (thickness = 72 nm), and (GeS₂)_{0.5}(Ag₂S)_{0.5} glass as the samples are heated. The data for the nanocomposites are labeled with their Ag₂S nanocrystal diameter. The data curve for the (GeS₂)_{0.5}(Ag₂S)_{0.5} glass is taken from reference [6]. The inset of part (c) shows a schematic of the measurement device.

matrix stoichiometry has strong implications for charge transport.^[32] Bychkov et al.^[28] varied the Ag atomic percent (at%) in bulk Ag-Ge-S by five orders of magnitude and found two separate transport regimes for ionic transport. For Ag < 2–5 at%, transport is dominated by conductive percolating pathways in an insulating glass, whereas for Ag > 10 at%, the glass itself begins to conduct. Since the precise stoichiometry of the nanocomposite’s sub-nanometer matrix cannot be measured, we refrain from speculating on its phase diagram location or transport regime. We do however note that the decomposition of ChaM clusters often results in chalcogen-deficiencies.^[5]

Resistance network arguments and the ionic conductivity trend with Ag₂S content lead us to believe that both the GeS₂ matrix and the Ag₂S nanocrystals have significant effects on the nanocomposite’s ionic conductivity. Based on the data in Figure 4b, we calculate the activation energies for ionic transport in the Ag₂S acanthite phase to be 0.64, 0.61, 0.76, and 0.70 eV for the pure Ag₂S film and composites with 4.3 nm, 7.0 nm, and 9.3 nm diameter nanocrystals, respectively. Due to the activation energy similarity between the pure Ag₂S and composites, it might seem reasonable to assume that the composite’s ionic resistance is completely dominated by the Ag₂S component. However, due to the nanocrystal–matrix geometry, the ionic transport through Ag₂S is both in series and in parallel with the GeS₂ matrix. In such a resistance network, it’s unlikely that the composite’s ionic resistance can be completely dominated by the Ag₂S component (see Supporting Information). Although the activation energies of the composites do not resemble that of a (GeS₂)_{0.5}(Ag₂S)_{0.5} glass, which is 0.31 eV,^[6] we note that the activation energy of Ag-Ge-S glasses are highly sensitive to stoichiometry; for example, the activation energy of (GeS₂)_{0.317}(GeS)_{0.633}(Ag₂S)_{0.05} glass is 0.68 eV.^[7] Consequently, we cannot assign an expected activation energy to the matrix because its precise stoichiometry is unknown. However, since we observe a strong dependence on the Ag₂S nanocrystal content, we can conclude that the matrix does not completely

dominate the composite’s ionic resistance. Since neither the Ag₂S component nor the GeS₂ component dominate the ionic resistance of the composite, we conclude that both components have a significant effect on the ionic conductivity of the composite.

Considering the trends in conductivity, we have demonstrated that varying the microstructure of Ag₂S nanocrystal–GeS₂ matrix composites permits systematic control of ionic and electronic transport. Notably, the ionic conductivity of the composites is enhanced relative to both pure Ag₂S and (GeS₂)_{0.5}(Ag₂S)_{0.5} glass. We also observed a temperature shift and thermal hysteresis in the Ag₂S phase transition temperature.

Experimental Section

Nanocomposite Preparation: Films of Ag₂S nanocrystals were prepared by drop-casting onto appropriately prepared substrates (see Supporting Information). After solvent evaporation, the nanocrystal films were briefly immersed in ethanol and then immersed in a solution of (N₂H₄)_x(N₂H₅)₄Ge₂S₆ ChaM clusters (100 mg) in ethanolamine (1.5 mL) for ~ 40 minutes. This step removes the octadecylamine ligands on the Ag₂S nanocrystals and replaces them with the ChaM clusters. The films were then immersed in ethanolamine for 10–15 seconds to remove excess ChaM clusters and then ethanol for another 10–15 seconds to rinse off ethanolamine. The amorphous GeS₂ matrix was made by heating the samples to 100 °C for 3 minutes and then 200 °C for 20 minutes, which decomposes the ChaM clusters. When a thicker film was desired, the above steps were repeated as necessary (typically two depositions in total). The nanocomposite films used for charge transport measurements were 200–600 nm thick. All nanocomposite preparation was done in a nitrogen-filled glove box.

XRD: Time-resolved XRD measurements were performed during rapid thermal annealing in a purified He atmosphere at beamline X20C of the National Synchrotron Light Source. The heating rate was 1 C s⁻¹. The annealing chamber is equipped with a boron nitride heater stage and the intensity of the XRD peaks is detected by a fast linear diode array detector that monitors the intensity of the XRD peaks over a 2θ range of 15°. The center of the detector was located at 2θ = 45° which allowed

the detection of strong Ag_2S diffraction peaks. The x-ray wavelength was 1.797 Å. Transition temperatures were determined by using the (121) and (022) diffraction peaks, which correspond to 40.34° and 40.71°, respectively. The diffracted intensity of these peaks was integrated over an angular range of 1°, and the inflection point of this integrated intensity curve was used to identify the transition temperature.

Charge Transport: An Agilent 4156C Precision Semiconductor Parameter Analyzer and an Agilent 4294a Precision Impedance Analyzer were used for dc and impedance spectroscopy measurements, respectively. Dc measurements were done by applying a 5 mV bias across the sample for 10 minutes. At steady state during the dc measurement, the platinum electrodes block the ionic current and the measured resistance corresponds to the electronic resistance, R_e . Impedance spectra were taken from 40 Hz to 50 MHz using an ac bias of 5 mV_{rms}. The resulting impedance spectra were fit with a model (see Supporting Information) to determine the high frequency impedance limit, which corresponds to $(R_e^{-1} + R_i^{-1})^{-1}$, where R_i is the ionic resistance. The impedance spectroscopy and dc measurements were done using the same electrode pair; hence R_e and R_i were measured at identical locations on the same sample. The electrode pair formed a gap 14 μm in length and 2000 μm in width. We calculated the activation energy for ionic transport, E_a , by fitting our data to the expression: $\sigma_i = A \exp[-E_a/(k_b T)]$, where A and k_b are a numerical coefficient and Boltzmann constant, respectively. All charge transport measurements were done inside a nitrogen-filled glove box in the temperature range of 130 °C ≤ T ≤ 230 °C using a home-built thermal chamber. Additional details on the charge transport measurements can be found in the Supporting Information.

Supporting Information

Supporting Information is available from the Wiley Online Library or from the author. The Supporting Information includes additional experimental details, figures, and discussion.

Acknowledgements

Work at the Molecular Foundry was supported by the U.S. Department of Energy (DOE) under Contract No. DE-AC02-05CH11231, including support from the Laboratory Directed Research and Development Program (Dr. Tangirala), and a DOE Early Career Research Program grant (Dr. Milliron). Use of the National Synchrotron Light Source, Brookhaven National Laboratory, was supported by the U.S. Department of Energy, Office of Science, Office of Basic Energy Sciences, under Contract No. DE-AC02-98CH10886.

Received: July 8, 2011

Revised: October 18, 2011

Published online: December 6, 2011

- [1] M. Balakrishnan, M. N. Kozicki, C. D. Poweleit, S. Bhagat, T. L. Alford, M. Mitkova, *J. Non-Cryst. Solids* **2007**, 353, 1454.
- [2] R. Waser, R. Dittmann, G. Staikov, K. Szot, *Adv. Mater.* **2009**, 21, 2632.
- [3] R. Tangirala, J. L. Baker, A. P. Alivisatos, D. J. Milliron, *Angew. Chem. Int. Ed.* **2010**, 49, 2878.
- [4] J. Park, J. Joo, S. G. Kwon, Y. Jang, T. Hyeon, *Angew. Chem. Int. Ed.* **2007**, 46, 4630.
- [5] D. B. Mitzi, *Adv. Mater.* **2009**, 21, 3141.
- [6] R. Belin, G. Taillades, A. Pradel, M. Ribes, *Solid State Ionics* **2000**, 136, 1025.
- [7] E. Robinel, B. Carette, M. Ribes, *J. Non-Cryst. Solids* **1983**, 57, 49.
- [8] H. Schmalzried, *Prog. Solid State Chem.* **1980**, 13, 119.
- [9] D. B. Mitzi, *Inorg. Chem.* **2005**, 44, 3755.
- [10] Y. Zoo, T. L. Alford, *J. Appl. Phys.* **2007**, 101, 033505.
- [11] M. D. Banus, *Science* **1965**, 147, 732.
- [12] V. D. Das, D. Karunakaran, *J. Appl. Phys.* **1989**, 66, 1822.
- [13] S. Banerjee, S. Bhattacharya, D. Chakravorty, *J. Phys. Chem. C* **2007**, 111, 13410.
- [14] R. Makiura, T. Yonemura, T. Yamada, M. Yamauchi, R. Ikeda, H. Kitagawa, K. Kato, M. Takata, *Nat. Mater.* **2009**, 8, 476.
- [15] S. K. Sharma, *J. Mater. Sci.* **1969**, 4, 189.
- [16] S. H. Tolbert, A. P. Alivisatos, *J. Chem. Phys.* **1995**, 102, 4642.
- [17] J. Jamnik, J. Maier, *J. Electrochem. Soc.* **1999**, 146, 4183.
- [18] W. Lai, S. M. Haile, *J. Am. Ceram. Soc.* **2005**, 88, 2979.
- [19] This estimate assumes a close-packed nanocrystal array with 0.7 nm of matrix material separating the nanocrystal edges.
- [20] C. Korte, N. Schichtel, D. Hesse, J. Janek, *Monatsh. Chem.* **2009**, 140, 1069.
- [21] I. Kosacki, C. M. Rouleau, P. F. Becher, J. Bentley, D. H. Lowndes, *Solid State Ionics* **2005**, 176, 1319.
- [22] A. Peters, C. Korte, D. Hesse, N. Zakharov, J. Janek, *Solid State Ionics* **2007**, 178, 67.
- [23] R. W. Schwartz, T. Schneller, R. Waser, *C. R. Chim.* **2004**, 7, 433.
- [24] N. Sata, K. Eberman, K. Eberl, J. Maier, *Nature* **2000**, 408, 946.
- [25] J. Maier, *Nat. Mater.* **2005**, 4, 805.
- [26] C. L. Li, X. X. Guo, L. Gu, D. Samuelis, J. Maier, *Adv. Funct. Mater.* **2011**, 21, 2901.
- [27] M. Ribes, E. Bychkov, A. Pradel, *J. Optoelectron. Adv. Mater.* **2001**, 3, 665.
- [28] E. Bychkov, V. Tsegelnik, Y. Vlasov, A. Pradel, M. Ribes, *J. Non-Cryst. Solids* **1996**, 208, 1.
- [29] O. L. Anderson, D. A. Stuart, *J. Am. Ceram. Soc.* **1954**, 37, 573.
- [30] S. R. Elliott, *J. Non-Cryst. Solids* **1994**, 172, 1343.
- [31] D. Ravaine, J. L. Souquet, *Phys. Chem. Glasses* **1977**, 18, 27.
- [32] M. Mitkova, Y. Wang, P. Boolchand, *Phys. Rev. Lett.* **1999**, 83, 3848.